Self-organized structure of vortex droplets in $Bi_2Sr_2CaCu_2O_8$ single crystals induced by ac magnetic field

L. S. Uspenskaya[1] and A. L. Rakhmanov[2]
[1]*Institute of Solid State Physics, Russian Academy of Sciences, Chernogolovka 142432, Russia*
[2]*Institute for Theoretical and Applied Electrodynamics, Russian Academy of Sciences, Moscow 125412, Russia*
(Received 22 January 2009; revised manuscript received 31 March 2009; published 27 April 2009)

In the paper [L. S. Uspenskaya and A. L. Rakhmanov, Phys. Rev. Lett. **100**, 137002 (2008)] we reported the magneto-optic observation of droplets of vortex matter in $Bi_2Sr_2CaCu_2O_8$ single crystals pumped by the low-frequency ac magnetic field. This self-organized structure grows along planar defects in the temperature range $12<T<30$ K. The droplet arises at some "weak" point in the defect, grows with number of periods of the ac field, "blows up," and shifts along the defect. Then, the next droplet arises at the same point. Here we present a detailed description of the phenomenon. In addition, we study evolution and relaxation of the droplets. The observed effect is interpreted in terms of the magnetic flux dynamics in the superconductor accounting for the energy of stray magnetic fields.

DOI: 10.1103/PhysRevB.79.144525 PACS number(s): 74.25.Qt, 74.72.Hs

I. INTRODUCTION

The dynamic of the magnetic flux in type-II superconductors is strongly nonlinear. This nonlinearity results from the repulsive interaction of the magnetic flux lines, interaction of the magnetic flux with the defects of the crystal structure, heating of a superconductor due to magnetic flux motion, etc. An additional source of nonlinear and nonlocal effects arises due to stray magnetic fields, which could not be ignored for the samples with a significant demagnetization factor, just like in the case of a ferromagnetic with a domain structure.[1] Under certain conditions, smooth magnetic flux penetration in a type-II superconductor can be violated by instabilities.[2] These instabilities result in the transition of the superconductor to resistive or even normal state and are of the first importance for the applications of superconductivity. On the other hand, the physics of instabilities in superconductors is very interesting and rich. It abounded with nontrivial nonstationary and nonuniform self-organized structures.

The thermomagnetic instabilities (flux jumps, normal zone propagation, etc.) were first observed in superconductors.[3,4] These types of instabilities were studied by many research groups since they limit the current-carrying capacity of superconducting wires in the important applications. In many cases, the development of the thermomagnetic instability is accompanied by the nonlinear field and temperature oscillations,[3,5] formation of moving domains,[4,5] and dendritelike penetration of the magnetic flux in the sample bulk.[6,7] The thermomagnetic instability does not exhaust all mechanisms giving rise to the formation of the self-organized nonstationary phenomena in the vortex matter in superconductors. The macroturbulent instability[8,9] or formation of twisters in $YBa_2Cu_3O_7$ (Ref. 10) as well as observation of flux droplets in $Bi_2Sr_2CaCu_2O_8$ (Bi2212) (Refs. 11 and 12) are not accompanied by a significant heating of the superconductor. However, these phenomena can be observed only if the sample temperature T is not low since the thermoactivation makes the flux lines mobile allowing them to overcome the pinning force.

In our previous paper[12] we reported the magneto-optic observation of a new type of the self-organized vortex matter structure in Bi2212 single crystals. We have observed the formation of macroscopical flux droplets in the low-frequency magnetic field transverse to the *ab* plane of the crystal. The droplet nucleates at some defect points, "breathes" with the field oscillation, growths with time, "blows up" and, finally, shifts to the sample bulk. Then, the next breather with the opposite flux polarization arises at the same point and so on. As a result, a beadlike structure (up to ten droplets) appears along the defect. The reported phenomenon resembles the effects of domain wall and the Bloch-line generation observed in the ferromagnetics[13] and irreversible flux pumping in type-I superconductors.[14] A different mechanism of pumping of the magnetic flux by ac field in Bi2212 single crystals was realized in experiments by Cole *et al.*[15] The flux quanta were guided using a drive that was asymmetric in time, in analogy with ratchet potential, which is asymmetric in space. In these experiments, the density of magnetic flux at the center of the sample was increased or decreased by varying the time asymmetry of the ac field. Note also that, in principle, the magnetic flux could be pumped in the center of superconducting sample by application of the coordinate-dependent ac drive due to arising of a so-called Kapitza potential.[16] Specific solitonlike structures pumped by ac magnetic field and commonly referred to as breathers were observed in Josephson-junction arrays.[17,18] Note that the described phenomenon in this paper has a different nature.

Here we reported more detailed study of the droplet pumping. Using new magneto-optical (MO) imaging data, we extracted the magnetic field distribution in the bulk sample and in the defect. We study the evolution of the magnetic flux and the evolution of the droplet appearance and size at different temperatures under different amplitude and frequency of the ac magnetic field. We study also a relaxation of the observed droplet structure after turning off the ac field analyzing both the MO images and the magnetic flux profiles along and across the defect. We observe the formation of the droplet pairs during the magnetic flux relaxation

in the sample. We find that the flux line droplets exist even after relaxation of all the flux lines in the sample bulk. A theoretical treatment of the observations is given in the framework of the suggested previously model.[12]

II. SAMPLES

The samples are high-quality Bi2212 single crystals having a form of thin plates with thickness of 30 μm along the **c** axis and sizes 3–4 mm in the **ab** plane. The current anisotropy J_{ab}/J_c is higher than 100. In the low-temperature range, $12<T<30$ K, the MO imaging demonstrates that the dc magnetic flux penetrates into the crystals homogeneously from each of the sample edges. The flux distribution is typical for high-quality crystals with almost constant critical current. The magnetic induction decreases monotonically from the sample edge to the bulk. The induction step near the surface[19] is on the order of the first critical field H_{c1}. The details of the sample properties can be found in Ref. 20. At higher temperatures, $T>30$ K, pinning in Bi2212 decreases drastically and the flux occupies the whole volume in tenths or even hundredths of seconds.[21,22]

The samples usually have few planar defects (parallel to **c** axis) typical for Bi2212 crystals. They are invisible in optics but become apparent in MO as weak links; at $T<30$ K the flux penetrates much deeper along these defects.[20]

III. EXPERIMENTAL

The observations are performed by high-resolution MO technique successfully used for visualization of the magnetic flux in the superconductors[23] in the temperature range of 12–90 K, in the transverse ac magnetic field with the amplitude H_a up to 1000 Oe, and in the frequency ω up to 10 kHz. The MO images were taken either by the EDC2000S digital camera of fixed sensitivity and variable exposure or by video camera Sony SSC DC50P. First camera enables us to capture the frames with exposure time down to 1ms with variable delay relative to the field phase; second one allows us to observe the development of the process in time, which gives a common pattern of excitation. The brightness of the MO images is a function of the magnetic induction. We calibrate the brightness with respect to the induction value. As a result, the profiles of the transverse magnetic induction along and across the defects were obtained. For more experimental details see Ref. 22.

IV. EXPERIMENTAL RESULTS

A. Flux penetration in dc field

As a first step we study the magnetic flux penetration into the sample placed in dc magnetic field. The typical MO imaging of the dc flux distribution is shown in Figs. 1(a)–1(d). Schematics of the crossing planar defects are depicted in Fig. 1(e). Images in Figs. 1(a)–1(d) are recorded in the increasing dc magnetic field varying from zero to $H_{dc}=457$ Oe. In this field range, the magnetic flux slightly penetrates the bulk of the sample near its edges while the vortices enter deep in the sample along the defects. Such a picture is typical for Bi2212

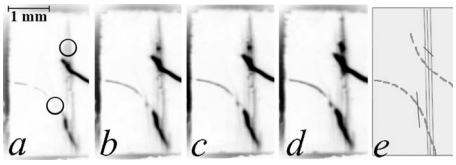

FIG. 1. MO images of Bi2212 single crystal in the dc magnetic field at $T=13$ K: images (a), (b), and (c) are taken in 5 s after turning on $H_{dc}=237$, 368, and 457 Oe, respectively; image (d) is taken in 20 s after turning on $H_{dc}=457$ Oe; and (e) is the schematic of planar defects. Dark regions show the places occupied by the magnetic flux. Circles in (a) indicate points of droplet formation in the ac magnetic field. Magnetic flux enters the sample deep along the defects and only slightly penetrates the sample bulk near the sample edges.

single crystals at low temperatures. Through the circles in Fig. 1(a) we also indicate the points of the droplet nucleation in the ac magnetic field.

Note that all these defect points are located on the planar defects passing through the sample. The MO images of the planar defects look like lines, which are the same on both sides of the single crystal. On these planar defects we observe some singular points in which the magnetic flux is captured under slow magnetization reversal of the sample. We believe that the specific nature of the defect is not of the first importance for the observation of the effect of the droplet pumping. Really, in our crystals there exist at any rate two types of the defects in which the generation of the droplet is found. We definitely identify a part of these singularities as crossing points of two planar defects and other points as crossing of the planar defect with a microscratch.

The relaxations of the magnetic induction profiles, $B(x_\alpha,t)$, are shown in Fig. 2 for different regions in the sample and along different directions x_α. The profiles are recorded from 5 to 300 s after turning on the dc field. As it is seen from these images, the screening current density along the sample edge is much larger than that across the defect. Correspondingly, the relaxation of the magnetic flux along the defect is much faster than near the edge and across the defect plane. The curves in Fig. 2(b) reveal that the magnetic flux accumulates in the "weak point."

The features of the dc field relaxation process are also illustrated in Figs. 3 and 4. The magnetic induction slowly decreases near the sample edge (circles in Fig. 3) due to the flux penetration in the sample bulk assisted by the thermoactivated flux creep (TAFF). On the contrary, the magnetic flux accumulates more rapidly in the "weak point" (triangles in Fig. 3). The gradients of the magnetic induction (or the densities of the corresponding screening currents) behave themselves in a very different manner in different sample points. The screening current gradually decays near the sample edges and along the defect far from the "weak point" due to the flux relaxation in the sample (see two lower groups of the experimental points in Fig. 4). At the same time, the screening current increases near the "weak point" in the direction across the defect and along it as well (see two upper groups of the experimental points in Fig. 4). The growth of the screening current is evidently arises due to the flux accumulation in the "weak point." In conclusion, the

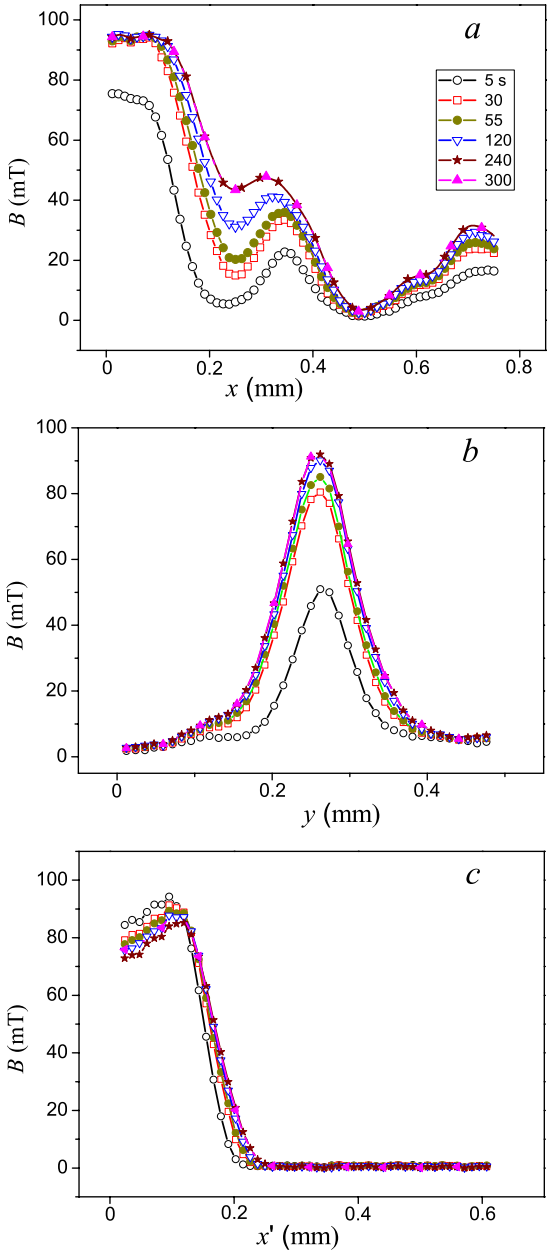

FIG. 2. (Color online) Magnetic induction profiles $B(x_\alpha,t)$ in the sample placed in the dc field H_{dc}=460 Oe at T=13 K in different moments of time from t=5 to 300 s; (a) induction profiles $B(x,t)$ along the planar defect; (b) induction profiles $B(y,t)$ across this defect at the "weak point," which corresponds the maximum at $x \approx 0.345$ mm in Fig. 2(a); and (c) typical induction profiles across the sample edge.

magnetic induction and the screening current density increase significantly (by a factor of about 2 for 5 min) near the "weak point."

B. Droplets pumping in ac field

Here we discuss the magnetic flux dynamics in the sample in the low amplitude (smaller than 1 kOe) ac magnetic field $H_a(t)$. In this amplitude range, the magnetic flux does not penetrate into the sample bulk except in areas near the edges

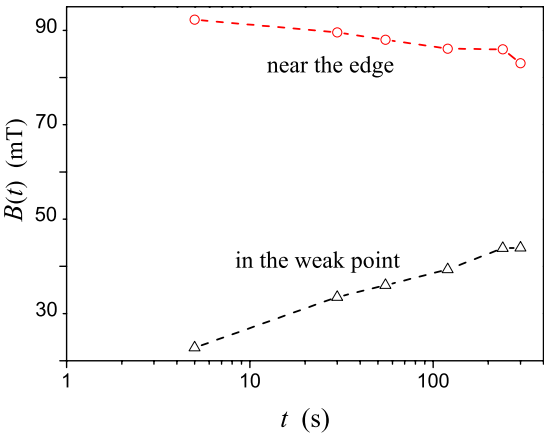

FIG. 3. (Color online) Evolution of the magnetic induction in the sample in the dc field H_{dc}=460 Oe at T=13 K: (red) circles: near the sample edge; (black) triangles: in the defect point.

and along the planar defects. The magnetic flux accumulates in the "weak point" at any frequency of the ac field ω if the flux penetration front in the defect is close to the intersection point with another defect ("weak point"). If the frequency of the ac field ω is small, $\omega < \omega_{min}$ (ω_{min} is about 10 Hz for our samples), the magnetic flux changes its sign in the "weak point," as well as in the other parts of the sample. The flux distribution after each ac field cycle is in many features similar to that observed in the dc field.

A distinct peculiarity in the magnetic flux distribution and dynamics is observed if ω exceeds the value ω_{min}.[12] In this case, the sign of the flux in the "weak point" remains unchanged during a number of the ac field cycles. Moreover, the flux and the value of the magnetic field induction $B(t)$ start to grow in this "weak point," and we observe that a flux droplet is pumped by the ac magnetic field. When the size of such droplet achieves a threshold value, some instability occurs, the droplet loses a part of its flux, and the next droplet

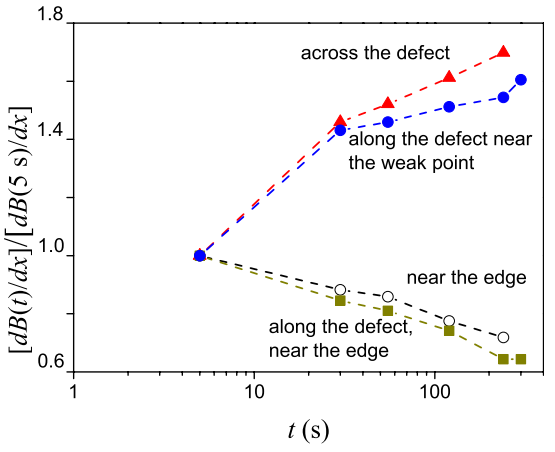

FIG. 4. (Color online) Relaxation of the induction gradient (or current density) normalized by its values at t=5 s: (red) triangles: across the defect at the "weak point;" (blue) circles: along defect at the "weak point;" (black) empty circles: near the edge; and (dark yellow) squares: along the defect far from the "weak point." The values of dc field and temperature are the same as in Fig. 3.

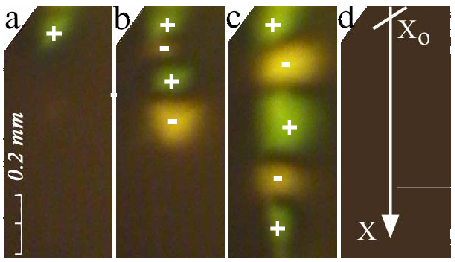

FIG. 5. (Color online) Nucleation of the flux droplets at "weak point;" $H_a=250$ Oe, $\omega=15$ Hz, and $T=18$ K; the nearest sample edge is on the top of the figures; (a) beginning of the droplet nucleation, (b) and (c) after many ac field cyclings, (d) schematic of the sample in the **ab** plane, magnetic field is along **c** axis, the "weak point" is located at $x=x_0$, and arrow indicates the planar defect position. Green (+) and yellow (–) droplets have opposite magnetic flux polarities.

with the opposite flux polarity begins to grow in the same point shifting the first droplet to the sample bulk along the defect. When the size of the second droplet achieves the critical value, the third droplet appears at the same point, and so on. As a result, a chain ("beads") of macroscopical flux droplets arises in the planar defect. This process is illustrated by MO images in Fig. 5. The dynamic picture of the droplet pumping is available online.[24] The effect is entirely reproducible and is observed at all "weak points" in the sample.

The magnetic flux enters the "weak point" if the polarity of the ac magnetic field coincides with the polarity of the flux in the droplet and a smaller amount of the vortices leaves the droplet if the polarities are different. As a result, the droplet "breathes" with the field oscillations: the MO image contrast and the droplet size increase if the sign of the external field coincides with the sign of the magnetic induction in the droplet and decrease if these signs differ (see MO images in Fig. 6). Thus, the flux droplets can be also referred to as the "breathers."

The evolution of the flux droplets with temperature is illustrated in Fig. 7. As it follows from the MO presented here, the droplet sizes increase with the temperature growth, their contours blur with approaching T to a threshold value of about 30 K, and at $T\gtrsim 30$ K the droplets were not observed.

The applied ac magnetic field pumps the flux droplets in a "weak point" if the flux penetration front occurs near this

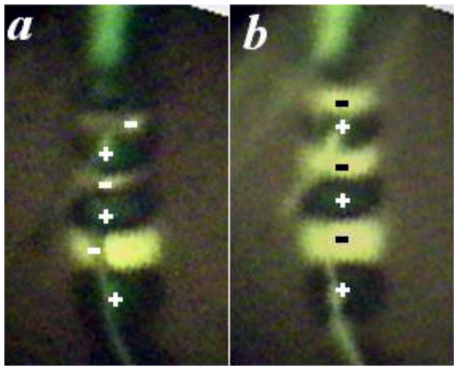

FIG. 6. (Color online) Droplet breathing: the left panel corresponds to $H_a(t)=H_a$, while the right panel corresponds to $H_a(t)=-H_a$.

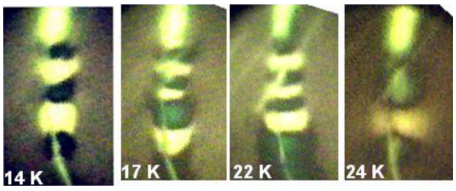

FIG. 7. (Color online) Evolution of the droplets appearance with increase in temperature.

point, that is, if the field amplitude H_a becomes larger than some threshold value $H_{\min}$, which is different for different "weak points." The nucleation of the droplets ceases if H_a exceeds a maximum value $H_{\max}$, when the amplitude of the droplet "breathing" becomes larger than the distance between the droplet at the "weak point" and the flux front. If $H_a>H_{\max}$, the vortices of the opposite polarity (antivortices) start to enter into the breather and it vanishes due to flux-antiflux annihilation. The amplitudes $H_{\max}$ and $H_{\min}$ depend on temperature and frequency: they decrease with T and increase with ω. The dependence of the threshold fields on temperature and frequency is illustrated in Figs. 8(a) and 8(b), respectively. As it is seen from Fig. 8(a), $H_{\min}=H_{\max}$ at $T\approx 29$ K and formation of droplets is not observed at higher temperatures. At low temperatures, the maximum and minimum field amplitudes are different. However, the effect disappears if $T\lesssim 12$ K.

As it was mentioned above, the pumping of the flux droplets is observed only within definite frequency and temperature ranges (see, e.g., Fig. 3 in Ref. 12). The pumping of the droplets is observed within the temperature $12\lesssim T\lesssim 30$ K and frequency $10\lesssim\omega\lesssim 300$ Hz ranges. At low temperatures, the magnetic flux motion is suppressed by strong pinning. On the contrary, if $T>30$ K, the pinning in Bi2212 becomes negligible; the flux lines move fast to the sample center and accumulate here.[20] In the range of the low frequencies, the magnetic flux dynamic in the samples is similar to the dc field case, while at high frequencies, the applied field changes its sign too fast and the pumping of the breather becomes inefficient.

We also perform experiments in the inclined magnetic field. We do not find any significant difference in the droplet nucleation depending on the direction of the inclined field or on the particular type of the defect region. If the inclination angle exceeds 20° the droplet generation ceases.

C. Droplets relaxation

In this section we discuss relaxation of the observed flux structures under turning off the ac magnetic field. For this goal, we first pumped the droplet structure by ac magnetic field with a fixed amplitude H_a and then decreased linearly the amplitude up to zero during 20–40 s. We recorded the MO images and extracted the magnetic induction profiles during diminishing of H_a and after turning off the ac field. Typical MO images of evolution of the droplet structure in such process are shown in Fig. 9 for two different ac field amplitude and frequencies.

The structure in Fig. 9(a) is pumped by ac field with the amplitude $H_a=350$ Oe and the frequency of 86 Hz. The am-

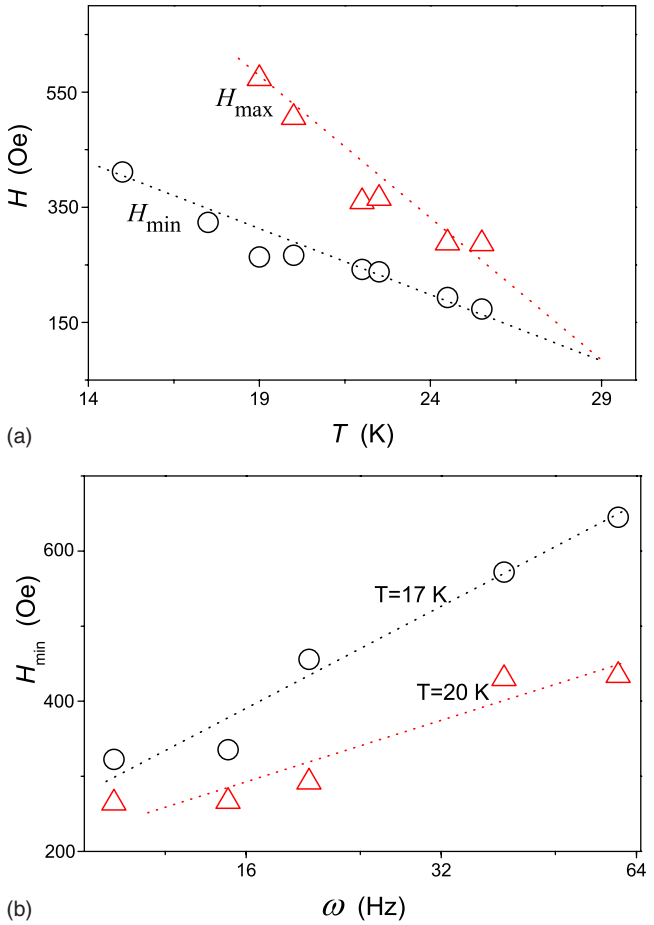

FIG. 8. (Color online) (a) Dependence of H_{max} (triangles) and H_{min} (circles) on T for the same "weak point" as in Fig. 1 at $\omega=15$ Hz. Lines are guides for eyes. (b) Dependence of H_{min} on ω at $T=17$ (circles) and 20 K (triangles). Lines are calculated using fitting parameters $x_s(10\ \text{Hz})/x_{min}=0.1$ and $n=2.7$ (see the text).

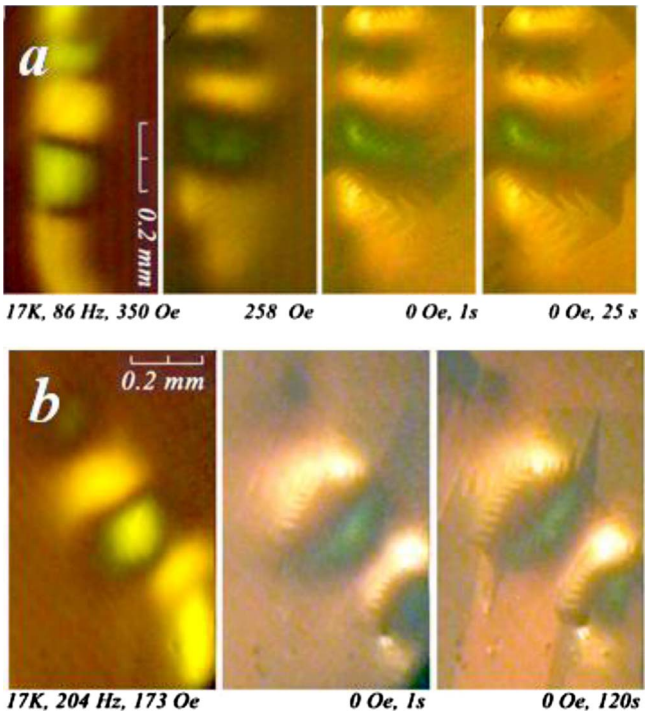

FIG. 9. (Color online) The set of the MO images of the droplets in the decreasing ac magnetic field and after turning off the field at $T=17$ K: the amplitude of the ac magnetic field H_a is decreased linearly to zero during 30 s; (a) $H_a=350$ Oe and $\omega=86$ Hz; (b) $H_a=173$ Oe and $\omega=204$ Hz.

plitude of the ac field is decreased linearly to zero during 30 s. Magnetic induction in the droplet continues to increase at the first stage of the amplitude decrease; however, this growth becomes slower and stops when $H_a \approx 300$ Oe. With the further decrease in the ac field amplitude, the droplets remain practically unchanged after a short and slow period of relaxation. At lower initial amplitudes and higher frequencies of the ac field [Fig. 9(b)], the behavior of the system is different. The droplet pumping stops just after decrease in H_a by a small value [by about 0.5 Oe under conditions of the experiment shown in Fig. 9(b)]. Then, the relaxation of the droplets is also very slow and the droplets are practically unchanged for about 120 s. In some of our experiments we wait 15 min and do not observe a significant droplet relaxation. In both cases shown in Fig. 9 the sizes of different droplets are equalized during the decrease in the ac field amplitude and, when the ac field is turned off, the droplets join in pairs consisting of two units with different polarities.

In Fig. 10, the profiles of the magnetic field along the linear defect are shown in different moments of time. The profiles are recorded from the sample edge ($x=0$) to the bulk through a single pumped large droplet. When the ac field amplitude starts to decrease, the magnetic induction in the droplet slightly diminishes and its distribution becomes asymmetrical. After the ac field is turned off, the relaxation rate of the magnetic flux in the "weak point" drops down drastically. The magnetic flux in the sample practically dis-

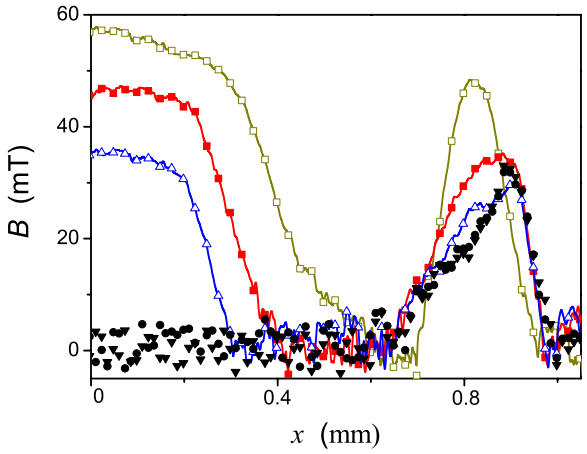

FIG. 10. (Color online) The relaxation of the profile of the magnetic field along the defect with a single pumped droplet ($T=17$ K, $\omega=60$ Hz, and the amplitude of the ac magnetic field decreases from 433 Oe to zero during 30 s); line with empty squares corresponds to the start of the amplitude decrease, line with filled squares corresponds to $H_a=340$ Oe, line with up empty triangles was recorded when $H_a=245$ Oe, filled circles correspond the first second when $H_a=0$, and filled down triangles were recorded after 120 s of the ac field turning off.

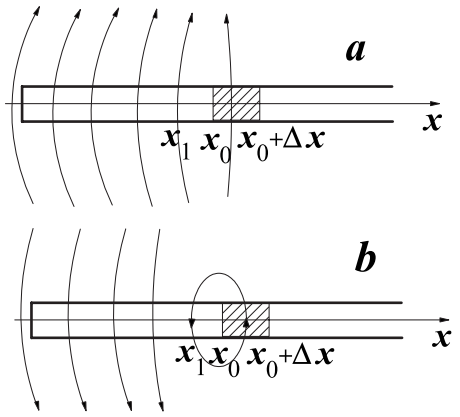

FIG. 11. Stray magnetic field distribution near the "weak point" at $x=x_0$ and entering flux front boundary at $x=x_1$: (a) the polarities of the entering flux and the induction in the droplet are the same: flux-flux case; (b) the polarities of the entering flux and the induction in the droplet are opposite: flux-antiflux case.

appears in 1 s after turning off the ac magnetic field—except for the magnetic flux in the droplet. This effect is observed in all our experiments with the magnetic flux relaxation. The droplet chains disappear by a jump when we heat the sample above $T=30$ K.

V. DISCUSSION

The mechanism that can describe the observed dynamics of the flux line structures was outlined in our previous paper.[12] Here we discuss it in more detail. We consider magnetic induction B_v produced by vortices penetrating a planar defect. The induction B_v depends on the coordinate x along the defect and time t and is zero outside the defect region. A screening current flows along the defect and across it near the flux penetration boundary. We describe the "weak point" existing at the crossing point between considered defect and some other defect as a local spot with strongly suppressed superconductivity. We denote the coordinate of the crossing point between the planar defect and the sample edge as $x=0$. The region with the suppressed superconductivity ("weak point") is located at $x_0<x<x_0+\Delta x$ (Fig. 11). We denote the position of the magnetic flux front at given value of the ac field amplitude H_a as $x_1(H_a)$. We consider here the case when the flux front is close to the "weak point" boundary at $x=x_0$.

In the first cycle of the applied magnetic field alternation, some vortices enter the region with suppressed superconductivity due to the TAFF and are captured here. The TAFF occurs as a thermally activated motion of the flux line bundles.[25] The TAFF escape rate is proportional to $\exp(-\Delta U/k_BT)$, where ΔU is the potential barrier that the flux bundle should overcome to hop from point x_1 to x_0 and k_B is the Boltzmann constant. The flux bundle entering the weak spot gains a potential energy $-U$. Then, the potential barrier that the flux bundle has to overcome to exit the weak spot is $\Delta U+U$. The captured vortices will be accumulated in the droplet if $U \gg k_BT$. When the external magnetic field changes its sign, "antivortices" enter the sample, and the boundary of "antiflux" is located evidently near the same point x_1 and the antivortices can hop from the point x_1 to the weak region at $x=x_0$ due to TAFF. The entering of the "antiflux" gives rise to the magnetic flux annihilation in the "weak point," which prevents the flux droplet growth. We can conclude that the breathers are pumped by the ac field if the potential barrier ΔU_f for the hopping of the flux lines with the same polarization as earlier captured in the weak spot is lower than the barrier ΔU_a for the flux lines with opposite polarity.

A. Potential barrier

The barrier ΔU consists of three terms. The first term comes from the pinning force (U_p), the second term is due to persistent currents flowing between the entering flux front and the vortices captured in the weak region (U_v), and the third contribution (U_m) is due to the energy of the stray magnetic fields arising due to nonzero demagnetization factor of the sample.

The pinning contribution U_p is independent of the mutual polarities of the magnetic induction in the droplet and in the entering flux and cannot be responsible for the droplet growth or decay. This term rapidly increases with the distance between the flux front and the "weak point," x_0-x_1, and the observation of the breather pumping is possible only if this distance is not large. Thus, the value of U_p is of importance for the observed phenomenon since it affects the minimum ac magnetic field amplitude.

The contribution to the energy barrier U_v, which arises due to the interaction of the flux lines with the screening currents, includes, in particular, the interaction between vortices. This interaction is repulsive for the "flux-flux" and attractive for the "flux-antiflux" configurations. The interaction between vortices stimulates entering the "antiflux" to the droplet and prevents flux pumping. However, the interaction between the vortices decays exponentially in the scale on the order of the London penetration depth in the *ab* plane, λ_{ab}. For Bi2212, this value is on the order of 200 nm. In our experiments, the characteristic distance x_0-x_1 between the flux front and the "weak point" is on the order of 0.02–0.2 mm, as it follows from the data shown in Figs. 2(a) and 10, which is almost 2–3 orders of magnitude larger than λ_{ab}. We can easily estimate U_v numerically in the London approximation using the approach to the flux interaction proposed in Ref. 26. For magnetic field and temperature ranges characteristic of our experiments, the difference in U_v for the "flux-flux" and "flux-antiflux" configurations becomes negligible (much smaller than k_BT) if x_0-x_1 is larger than the London penetration depth λ_{ab} in the **ab** plane by a factor of $2 \div 2.5$. Thus, the difference for the "flux-flux" and "flux-antiflux" cases in term U_v can be safely neglected in all further considerations.

The potential barrier U_m arising due to the stray fields depends on the mutual polarity of the flux in the droplet and of the entering flux since the stray fields near the sample surface are different for the "flux-flux" and "flux-antiflux" cases as illustrated in Fig. 11. A superconductor is diamagnetic material, and the magnetization of the sample decreases with the entering of the magnetic flux. Hence, the stray field

term U_m is negative giving rise to the barrier lowering. The entering of the flux into the droplet results in the decrease in the total sample magnetization, while the hopping of the antiflux reduces the magnetic induction in the droplet and is less favorable energetically. In other words, for the "flux-antiflux" configuration [Fig. 11(b)] the pattern of the magnetic field lines is similar to that near domain wall in the ferromagnetic. Due to thermoactivated hopping of the antiflux into the droplet, the stray magnetic field varies in the space on the order of x_0-x_1 in the transverse to the sample plane (z) direction. In the case of the "flux-flux" configuration [Fig. 11(a)] the magnetic field changes in a space with transverse dimension of the sample width and the energy gain due to TAFF are larger. Thus, the energy barrier is lower for the "flux-flux" configuration. This gives rise to the breather pumping in the ac field.

To illustrate these speculations, we consider the following simplified problem. We assume that the magnetic field configurations for the "flux-flux" and "flux-antiflux" cases are similar except the region near the "weak point." We denote these similar parts of the magnetic field in the sample and ambient space as $\mathbf{H}_0(\mathbf{x})$. The magnetic flux captured in the "weak point" produces the field $\pm\mathbf{H}_{\rm in}(\mathbf{x})$, where plus corresponds to the "flux-flux" and minus "flux-antiflux" cases, respectively. The Gibs free energy for these cases reads as

$$\mathcal{F}=\int_V dV\left\{\frac{[\mathbf{H}_0(\mathbf{x})\pm\mathbf{H}_{\rm in}(\mathbf{x})]^2}{8\pi}-\frac{[\mathbf{H}_0(\mathbf{x})\pm\mathbf{H}_{\rm in}(\mathbf{x})]\mathbf{H}_a}{4\pi}\right\}, \tag{1}$$

where the upper and lower signs correspond to the "flux-flux" and "flux-antiflux" configurations, respectively, $\mathbf{H}_a$ is the external field, $\mathbf{H}_a=\mathbf{H}_0(\mathbf{x})$ at $|\mathbf{x}|\to\infty$, and integration is performed over the total space including sample volume.

We analyze two identical processes. A small flux $\delta\Phi$ moves from the point at x close to x_1 to the "weak point." The magnetic fields in the sample and ambient volume vary by small values $\delta\mathbf{H}_{\rm ff}(\mathbf{x})$ or $\delta\mathbf{H}_{\rm af}(\mathbf{x})$ in the case "flux-flux" or "flux-antiflux" configurations, respectively. The resulting magnetic field distributions are $\mathbf{H}_0+\mathbf{H}_{\rm in}+\delta\mathbf{H}_{\rm ff}$ and $\mathbf{H}_0-\mathbf{H}_{\rm in}+\delta\mathbf{H}_{\rm af}$. Thus, the contributions U_m to the potential barrier for these two configurations are

$$U^m_{\rm ff}=\mathcal{F}_{\rm ff}(\mathbf{H}_0,\mathbf{H}_{\rm in},\delta\mathbf{H}_{\rm ff})-\mathcal{F}_{\rm ff}(\mathbf{H}_0,\mathbf{H}_{\rm in},0),$$

$$U^m_{\rm af}=\mathcal{F}_{\rm af}(\mathbf{H}_0,\mathbf{H}_{\rm in},\delta\mathbf{H}_{\rm af})-\mathcal{F}_{\rm af}(\mathbf{H}_0,\mathbf{H}_{\rm in},0). \tag{2}$$

We subtract the second barrier from the first one and neglect small quadratic terms with respect to the magnetic field changes. As a result, we derive from Eqs. (1) and (2) after simple calculations,

$$U^m_{\rm ff}-U^m_{\rm af}\approx\int_V\frac{dV}{4\pi}[\mathbf{H}_{\rm in}(\delta\mathbf{H}_{\rm ff}+\delta\mathbf{H}_{\rm af})-(\mathbf{H}_a-\mathbf{H}_0)(\delta\mathbf{H}_{\rm ff}-\delta\mathbf{H}_{\rm af})].$$

As it was mentioned in the beginning of this subsection,

$$\left|\int_V\frac{dV}{4\pi}\delta\mathbf{H}_{\rm ff}\right|\gg\left|\int_V\frac{dV}{4\pi}\delta\mathbf{H}_{\rm af}\right|$$

[compare Figs. 11(a) and 11(b)]. The value,

$$\left|\int_V\frac{dV}{4\pi}(\mathbf{H}_a-\mathbf{H}_0)\right|,$$

is on the order of the total diamagnetic moment of the sample and is much larger than the corresponding contribution due to small $H_{\rm in}$. Therefore, the difference $U^m_{\rm ff}-U^m_{\rm af}$ is evidently negative. Therefore, the potential barrier for the activated flux is lower in the case of the "flux-flux" configuration, which gives rise to the droplet pumping. In Ref. 12 this fact was illustrated numerically for a specific case of the flux activation.

B. Model for current distribution and relaxation

As in our previous paper,[12] we approximate the magnetic induction distribution in the sample following a standard approach used for solving magnetostatic problems.[27] We approximate the sample by an effective ellipsoid with the demagnetization factor β.[27] In this approximation, the magnetic field at the sample edge is

$$H(0)=H_a(t)/(1-\beta). \tag{3}$$

We denote the effective defect thickness as d. We neglect the y dependence of the induction in the defect and put in integrals $B_v(x,y)=dB_v(x)\delta(y)$, where $\delta(y)$ is the delta function and y is the defect position. We approximate as a steplike function the magnetic induction in the weak spot $B_{\rm in}(x)$, which is $B_{\rm in}(x)=B_{\rm in}$ within the spot, $x_0<x<x_0+\Delta x$ and $B_{\rm in}(x)=0$ outside it. At $x<x_1$, we can write

$$B_v(x,y)=\left[\frac{H_a}{1-\beta}-H_s-\frac{4\pi}{c}\int_0^x j(E)dx\right]d\delta(y), \tag{4}$$

where $x=0$ corresponds to the sample edge, H_s is the induction jump near the sample edge, j is the current density, and E is the electric field. We ignore the magnetic field dependence of j and will use the current-voltage characteristics in the form $j(E)=j_0(E/E_0)^{1/n}$ with $n>1$, which is usual for type-II superconductors.[25]

The TAFF relaxation time is $\tau_r\sim\omega_0^{-1}\exp(\Delta U/k_BT)$, where ω_0 is a characteristic frequency. If $\omega\tau_r\gg1$, the electric field E is determined mainly by the ac field variation rate. In this case, we can apply Bean's critical state model, $j\approx j_c$, with the critical current density $j_c=j(E(0))=$const, where $E(0)$ is the electric field at the sample edge.[28] Equation (4) gives $x_1=c[H_a/(1-\beta)-H_s]/4\pi j_c$.

C. Amplitude, frequency, and temperature limits

The current changes its direction with the sign of the external field. This current alternation gives rise to the droplet "breathing." The droplet pumping can be observed if $U^m_{\rm fa}-U^m_{\rm ff}\gg k_BT$. The effect disappears at higher temperatures due to both the increase in k_BT and decrease in the absolute values of the barriers. The flux $\delta\Phi$ entering the droplet during a

cycle of the ac field is proportional to the ac field period and is inverse proportional to τ_r, $\delta\Phi \propto 1/\omega\tau_r$. Thus, $\delta\Phi$ decreases exponentially with the decrease in T and the effect disappears at low T. Therefore, the breather pumping exists within some temperature range $T_{\min} < T < T_{\max}$, as it is observed in the experiment [Figs. 3 and 8(a) in Ref. 12]. Similar considerations can be used for the frequency band. First, it is necessary that $\omega\tau_r \gg 1$ because otherwise the TAFF paints over the droplet pumping. Second, if $\omega\tau_r$ is too small then $\delta\Phi$ becomes also small and the difference $U^m_{\rm fa} - U^m_{\rm ff}$ becomes smaller than $k_B T$. Thus, the effect can exist within definite frequency range.[12]

The contribution U_p to the activation barrier increases with the increase in the distance between the "weak" point and the flux front, $x_0 - x_1$. Thus, the droplet pumping starts if the entering flux at x_1 is near the defect at x_0. Otherwise, $U_p \gg k_B T$ and the flux activation to the weak region is damped by pinning. We denote the minimum value of x_1 necessary for the effect observation as $x_{\min}$. Thus, the minimum ac field amplitude necessary for the droplet growth can be determined as

$$H_{\min} = (1-\beta)H_s(1 + x_{\min}/x_s), \tag{5}$$

where $x_s = cH_s/4\pi j_c \propto \omega^{-1/n}$. The curves $H_{\min}(\omega)$ calculated by means of Eqs. (4) and (5) are shown in Fig. 8(b) by dashed lines for fitting parameters $x_s(10\ \text{Hz})/x_{\min} = 0.1$ and $n = 2.7$.

The "vortex-antivortex" attraction becomes large if the flux front is close to the weak region, $x_0 - x_1 \lesssim \lambda$. In this case the droplet pumping is impossible. We denote the maximum value of the ac field amplitude as $H_{\max}$. Since $x_0 \gg \lambda$, we can write $H_{\max} = (1-\beta)H_s(1 + x_0/x_s)$. Thus, the function $H_{\max}$ depends on ω through the same value $x_s \propto \omega^{-1/n}$. The temperature dependence of $H_{\min}$ and $H_{\max}$ is due to the temperature dependence of the critical current j_c. The experimental curves in Fig. 8(a) can be fitted if we put $j_c \propto 1 - T/T_{\rm dp}$, where $T_{\rm dp} \approx 30$ K is the depinning temperature, $(1-\beta)H_s \approx 150$ Oe, and $x_0/x_{\min} \approx 2$.

With the increase of the field in the droplet $H_{\rm in}$, the vortex energy gain in the weak region becomes smaller due to the vortex-vortex repulsion, which is proportional to $H^2_{\rm in}$. At some threshold field in the "weak point" $H_{\rm in} = H_{\rm thr}$, the potential minimum disappears. In other terms, this occur when the superconducting current is unable to screen the captured flux in the "weak point." One can expect that $H_{\rm thr}$ is on the order of the magnetic field at the sample edge at which the flux penetration into the defect begins. This agrees with the experiment. If $H_{\rm in} > H_{\rm thr}$, the breather becomes unstable and a part of the flux moves along the defect toward the sample bulk. At the next stage, the droplet with the flux of the opposite sign starts to grow in the weak region since the system of droplets with alternating flux polarity has lower energy than the chain with the same or random flux polarity.

VI. CONCLUSIONS

In conclusion, we present here a detailed description of the flux droplet pumping in Bi2212 single crystals placed in the low-frequency ac magnetic field first reported in Ref. 12. This effect exists in a definite range of temperature, ac field frequency, and amplitude. The droplet pumping arises due to the demagnetization factor of the sample. The accumulation of the flux in "weak points" of the sample in ac magnetic field becomes favorable due to decrease in energy of the stray magnetic fields near the sample surface. It is interesting to note that the droplet structures in the defects are very stable. For example, the chain of droplets remains practically unchanged in the defect for several minutes after turning off the ac field while the flux abandons other parts of the sample (including defects) much faster (about 1 s). The observed droplet is an example of the self-organized structures arising in the vortex matter. This phenomenon can be of importance for applications of Bi2212 superconductors since it provides an additional mechanism of dissipation in ac magnetic field.

ACKNOWLEDGMENTS

The work was supported by RFBR (Grants No. 09-02-00856 and No. 09-02-00248).

[1] P. G. De Gennes, *Superconductivity of Metals and Alloys* (Westview, Reading, MA, 1999).

[2] E. R. Nowak, O. W. Taylor, L. Liu, H. M. Jaeger, and T. I. Selinder, Phys. Rev. B **55**, 11702 (1997); C. J. Olson, C. Reichhardt, and F. Nori, *ibid.* **56**, 6175 (1997); E. Altshuler and T. H. Johansen, Rev. Mod. Phys. **76**, 471 (2004).

[3] R. G. Mints and A. L. Rakhmanov, Rev. Mod. Phys. **53**, 551 (1981).

[4] A. Vl. Gurevich and R. G. Mints, Rev. Mod. Phys. **59**, 941 (1987).

[5] V. R. Misko, S. Savel'ev, A. L. Rakhmanov, and F. Nori, Phys. Rev. Lett. **96**, 127004 (2006); Phys. Rev. B **75**, 024509 (2007).

[6] P. Leiderer, J. Boneberg, P. Brüll, V. Bujok, and S. Herminghaus, Phys. Rev. Lett. **71**, 2646 (1993); I. A. Rudnev, D. V. Shantsev, T. H. Johansen, and A. E. Primenko, Appl. Phys. Lett. **87**, 042502 (2005).

[7] A. L. Rakhmanov, D. V. Shantsev, Y. M. Galperin, and T. H. Johansen, Phys. Rev. B **70**, 224502 (2004); D. V. Denisov, A. L. Rakhmanov, D. V. Shantsev, Y. M. Galperin, and T. H. Johansen, *ibid.* **73**, 014512 (2006).

[8] V. K. Vlasko-Vlasov, V. I. Nikitenko, A. A. Polyanskii, G. W. Crabtree, U. Welp, and B. W. Veal, Physica C **222**, 361 (1994); T. Frello, M. Baziljevich, T. H. Johansen, N. H. Andersen, Th. Wolf, and M. R. Koblischka, Phys. Rev. B **59**, R6639 (1999).

[9] L. M. Fisher, P. E. Goa, M. Baziljevich, T. H. Johansen, A. L. Rakhmanov, and V. A. Yampol'skii, Phys. Rev. Lett. **87**, 247005 (2001); L. M. Fisher, A. Bobyl, T. H. Johansen, A. L. Rakhmanov, V. A. Yampolskii, A. V. Bondarenko, and M. A. Obolen-

skii, *ibid.* **92**, 037002, (2004).
[10] M. V. Indenbom, C. J. van der Beek, V. Berseth, V. V. Benoit, G. D'Anna, A. Erb, E. Walker, and R. Flükiger, Nature (London) **385**, 702 (1997); L. S. Uspenskaya and D. N. Kontuganov, Physica C **460-462**, 1288 (2007).
[11] L. S. Uspenskaya, I. G. Naumenko, and A. A. Zhokhov, Physica C **402**, 188 (2004).
[12] L. S. Uspenskaya and A. L. Rakhmanov, Phys. Rev. Lett. **100**, 137002 (2008).
[13] H. Dötsch and H. J. Schmitt, J. Appl. Phys. **24**, 442 (1974); V. I. Nikitenko, L. M. Dedukh, V. S. Gornakov, and Yu. P. Kabanov, JETP Lett. **32**, 377 (1980); V. K. Vlasko-Vlasov and L. S. Uspenskaya, Zh. Eksp. Teor. Fiz. **91**, 1494 (1986); V. K. Vlasko-Vlasov and L. S. Uspenskaya, *ibid.* **100**, 944 (1992).
[14] V. T. Dolgopolov and S. S. Murzin, Sov. Phys. JETP **46**, 1195 (1977).
[15] D. Cole, S. Bending, S. Savel'ev, A. Grigorenko, T. Tamegai, and F. Nori, Nat. Mater. **5**, 305 (2006).
[16] L. D. Landau and E. M. Lifshitz, *Mechanics* (Pergamon, Oxford, 1976), pp. 93–95; P. L. Kapitza, Zh. Eksp. Teor. Fiz. **21**, 588 (1951).
[17] E. Trias, J. J. Mazo, and T. P. Orlando, Phys. Rev. Lett. **84**, 741 (2000); P. Binder, D. Abraimov, A. V. Ustinov, S. Flach, and Y. Zolotaryuk, *ibid.* **84**, 745 (2000).
[18] E. Trias, J. J. Mazo, and T. P. Orlando, Phys. Rev. B **65**, 054517 (2002).
[19] E. H. Brandt and M. V. Indenbom, Phys. Rev. B **48**, 12893 (1993).
[20] M. V. Indenbom, C. J. van der Beek, V. Berseth, T. Wolf, H. Berger, and W. Benoit, J. Low Temp. Phys. **105**, 1529 (1996); I-Fei Tsu, Jyh-Lih Wang, S. E. Babcock, A. A. Polyanskii, D. C. Larbalestier, and K. E. Sickafus, Physica C **349**, 8 (2001).
[21] M. V. Indenbom, G. D'Anna, M.-O. Andre, V. V. Kabanov, and W. Benoit, Physica C **235–240**, 201 (1994).
[22] L. S. Uspenskaya, A. B. Kulakov, and A. L. Rakhmanov, Phys. Rev. B **68**, 104506 (2003).
[23] Ch. Jooss, J. Albrecht, H. Kuhn, S. Leonhardt, and H. Kronmüller, Rep. Prog. Phys. **65**, 651 (2002); M. V. Indenbom, V. I. Nikitenko, A. A. Polyanskii, and V. K. Vlasko-Vlasov, Cryogenics **30**, 747 (1990); L. S. Uspenskaya, V. K. Vlasko-Vlasov, V. I. Nikitenko, and T. H. Johansen, Phys. Rev. B **56**, 11979 (1997).
[24] http://www.issp.ac.ru/lrsc/usp/droplets.html
[25] G. Blatter, M. V. Feigel'man, V. B. Geshkenbein, A. I. Larkin, and V. M. Vinokur, Rev. Mod. Phys. **66**, 1125 (1994).
[26] J. R. Clem, J. Low Temp. Phys. **18**, 427 (1975).
[27] L. D. Landau, E. M. Lifshitz, and L. P. Pitaevskii, *Electrodynamics of Continuous Media* (Butterworth-Heinemann, Oxford, 1995).
[28] This result is confirmed by direct numerical calculations if $n \gtrsim 2.5-3$.